

Three-dimensional Microlensing

Shude Mao^{1,2}, Hans J. Witt³ and Jin H. An¹

¹ National Astronomical Observatories, 20A Datun Road, Chinese Academy of Sciences, Beijing, 100012, China

² Jodrell Bank Centre for Astrophysics, The University of Manchester, Alan Turing Building, Manchester M13 9PL, UK

³ Im Hollergrund 76, 28357 Bremen, Germany

Accepted Received ; in original form.....

ABSTRACT

We study three-dimensional microlensing where two lenses are located at different distances along the line of sight. We formulate the lens equation in complex notations and recover several previous results. There are in total either 4 or 6 images, with an equal number of images with positive and negative parities. We find that the sum of signed magnifications for six image configurations is unity. Furthermore, we show that the light curves can be qualitatively different from those for binary lensing in a single plane. In particular, the magnifications between a ‘U’-shaped caustic crossing can be close to unity, rather than having a minimum magnification of 3 as in the single plane binary lensing. There is only a small probability three-dimensional microlensing events will be seen in microlensing toward the Galactic centre. It is more likely they will be first seen in cosmological microlensing.

Key words: Gravitational lensing: micro - Gravitational lensing: strong - Galaxy: structure - Galaxy: bulge - Galaxy: centre

1 INTRODUCTION

Most gravitational lensing studies assume the thin lens approximation where all the mass distribution is collapsed into a single plane. Erdl & Schneider (1993) first provided a complete classification of the critical curves and caustics for two point lenses at different distances. The critical curves, caustics and bounds on the number of images of N point lens in multiple planes have been further studied using Morse theory (Levine, Petters & Wambsgans 1993; Petters 1995a,b, 1997; Petters & Wicklin 1995). The magnification probability distribution due to lenses in multiple planes has also been explored by Pei (1993) and Lee et al. (1997).

For lensing by galaxies (rather than by point lenses such as stars), Kochanek & Apostolakis (1988) first studied two-plane lensing, and concluded that 10% of gravitational lenses may be due to multiple-plane lensing. This is roughly consistent with the CLASS survey statistics within which one lens out of ~ 20 was found to be due to two galaxies at different redshifts (Browne et al. 2003; Chae, Mao & Augusto 2001). Werner, An & Evans (2008) studied the number of rings formed by lenses in two different planes, concluding there are at maximum three rings in general. Models have also been proposed for specific lenses, for example, Chae et al. (2001) studied the case for B2114+022 (Augusto et al. 2001) while Mihov (2001) presents a two-plane lens model for the system Q2237+0305.

These previous studies concentrated on image numbers, critical curves and caustics except Pei (1993) and Lee et al. (1997). In this work, we shall study the light curves due to three-dimensional microlensing. We first recast the lens equations into complex form, and found new derivations in terms of caustics and critical curves.

We then study the light curves in two point lens microlensing, find some qualitatively different features in the light curve (see also Lee et al. 1997) and provide some analytic insights into the behaviour.

The structure of the paper is as follows: in §2, we outline the theory of three-dimensional microlensing, in §3 we show examples of light curves, and in §4 we then discuss how such effects may be observable in Galactic and cosmological microlensing.

2 THEORY

The basic formalism of three-dimensional microlensing for two-point lenses are spelt out by Erdl & Schneider (1993). Following their approach, we align the optical axis with the line from the observer to the nearest point lens, that is, the first lens is at the origin $(0, 0)$. The first lens has mass M_1 and is at distance D_1 ; the second, farther-away lens has mass M_2 at distance D_2 ($D_1 \leq D_2$). In complex notations, the lens equation can be written as

$$w = z - \frac{\beta m_1}{\bar{z}}, \quad z_s = z - \frac{m_1}{\bar{z}} - \frac{m_2}{\bar{w} - \bar{z}_2}, \quad (1)$$

where again the first lens is set at the origin, z_2 is the second lens position (in principle, we can put the second lens on the x -axis without any loss of generality and then $z_2 = \bar{z}_2$), w is where the light ray lands on the second lens plane, z_s is the source position, m_1 and m_2 are scaled lens masses with

$$m_1 \equiv \frac{M_1}{M_1 + \alpha M_2}, \quad m_2 \equiv 1 - m_1, \quad (2)$$

and

$$\alpha \equiv \frac{D_1 D_{2s}}{D_{1s} D_2}, \quad \beta \equiv \frac{D_{12} D_s}{D_{1s} D_2}. \quad (3)$$

The lengths are normalised to the Einstein radius

$$r_E = \sqrt{\frac{4GD_{1s}D_1}{c^2}(M_1 + \alpha M_2)}, \quad (4)$$

and all the distances have their usual definitions, e.g., D_{1s} is the distance from the first lens to the source, D_1 is the distance to the first lens, and D_s is the distance to the source.

Notice that the parameter β specifies how three-dimensional the system is. If the two lenses are in the same plane, then $\beta = 0$ ($\alpha = 1$), and the Einstein radius is simply that corresponding to the total mass $M_1 + M_2$. On the other hand, if $D_2 \rightarrow D_s$, $\alpha \rightarrow 0$, $\beta \rightarrow 1$ and the Einstein radius defined in eq. (4) is determined by M_1 only. In general, $0 \leq \beta \leq 1$.

In this paper we shall adopt Euclidean geometry which is applicable to microlensing in the Galaxy. In this case,

$$\beta = \frac{(d_2 - d_1)}{(1 - d_1)d_2}, \quad \alpha = 1 - \beta, \quad (5)$$

where we define

$$d_1 \equiv \frac{D_1}{D_s}, \quad d_2 \equiv \frac{D_2}{D_s}. \quad (6)$$

All our results can be trivially generalised to cosmological microlensing by adopting angular diameter distances, although $\alpha = 1 - \beta$ is no longer true.

2.1 Image positions

Eliminating \bar{w} from eq. (1) by means of inserting the complex conjugate of the first to the second results in

$$z_s = z - \frac{m_1}{\bar{z}} - \frac{m_2 z}{(\bar{z} - \bar{z}_2)z - \beta m_1}. \quad (7)$$

The image positions are thus found to be zeros of the polynomial,

$$f(z, \bar{z}) = (z\bar{z} - z_s\bar{z} - m_1)(z\bar{z} - \bar{z}_2 z - \beta m_1) - m_2 z \bar{z}. \quad (8)$$

Considered as independent variables, (z, \bar{z}) is then the simultaneous solution of two equations $f(z, \bar{z}) = \bar{f}(z, \bar{z}) = 0$. For the polynomial in eq. (8), the Bernstein theorem (Bernshtein 1975, see also Sturmfels 2002) indicates that there in general exist six non-zero complex solutions provided that none of $z_s, z_2, \beta, m_1, m_2$ is zero (there are five solutions if $\beta = 0$ whilst the number of non-zero solutions is four if either $z_s = 0$ or $z_2 = 0$). This is also verified more prosaically by further eliminating \bar{z} from eq. (7) using its complex conjugate. In principle we can achieve this by computing the resultant of $f(z, \bar{z})$ and $\bar{f}(z, \bar{z})$ considered as the polynomials of \bar{z} , which is easily done using any modern symbolic computer algebra software, e.g., MAPLETM or MATHEMATICA[®]. We then obtain the sextic polynomial of z , whose coefficients are given in Appendix A. Therefore the number of images for the lens system here is bounded above by six, which is in fact achieved when a source is inside caustics.

The lens system under consideration is localised, and so the images for $z_s \rightarrow \infty$ are obtained either for divergent bending angles, which formally occur when the light ray falls exactly on the lens, or for $z \rightarrow \infty$. Counting two solutions of $w = z_2$ as well as $z = 0$ and $z = \infty$, we then find that there must be four images as $z_s \rightarrow \infty$, which is the number of images for a source outside caustics. We also find that the images corresponding to $z \rightarrow \infty$ and $z \rightarrow 0$ respectively have the positive and the negative parity, whereas the parities of the two images for $w = z_2$ are opposite to each other. Since the index theorem for image parities still holds, a pair of images having opposite parities form or merge when the

source crosses caustics. Hence, we have always an equal number of positive and negative parity images (see Erdl & Schneider 1993).

2.2 Magnifications

Using external products, it is trivial to generalise the expression in Witt (1990) to the three-dimensional case to obtain (see Rhie 1997)

$$\det J = \partial z_s \bar{\partial} \bar{z}_s - \partial \bar{z}_s \bar{\partial} z_s; \quad (9)$$

$$\partial z_s = 1 + \frac{\beta m_1 m_2}{h^2}, \quad \bar{\partial} z_s = \frac{m_1}{\bar{z}^2} + \frac{m_2 z^2}{h^2}. \quad (10)$$

where $h \equiv z(\bar{z} - \bar{z}_2) - \beta m_1$ whilst $\partial z_s \equiv \partial z_s / \partial z$ and $\bar{\partial} z_s \equiv \partial z_s / \partial \bar{z}$ etc. (also note $\bar{\partial} z_s = \bar{\partial} \bar{z}_s$ and $\partial \bar{z}_s = \partial z_s$). The magnification of the image at z is then given by $\mu = (\det J)^{-1}$.

The critical curves are defined as the locus of $\det J = 0$, that is, $\partial z_s \bar{\partial} \bar{z}_s = \partial \bar{z}_s \bar{\partial} z_s$, which is also equivalent to $|\partial z_s| = |\partial \bar{z}_s|$ and $|\partial z_s / \partial \bar{z}_s| = 1$. We may then write a parametric representation of the critical curves

$$e^{2i\varphi} \partial z_s = \bar{\partial} \bar{z}_s, \quad e^{-2i\varphi} \bar{\partial} \bar{z}_s = \partial z_s. \quad (11)$$

We note the linearised lens mapping near the point on critical curves follows as

$$\delta z_s(\delta z) = \partial z_s \delta z + \bar{\partial} \bar{z}_s \delta \bar{z} = \left(1 + e^{2i\varphi} \frac{\delta \bar{z}}{\delta z}\right) \partial z_s \delta z, \quad (12)$$

and thus we find that $\delta z_s(e^{i\varphi}) = 0$ – that is, $e^{i\varphi} = e^{i(\varphi + \pi/2)}$ corresponds to the critical direction on the image plane. Note also that $\delta z_s(e^{i\varphi}) = 2e^{i\varphi} \partial z_s$, but here ∂z_s is not necessarily real. Hence the projection direction, $e^{i\varphi}$ mapped onto the source plane becomes rotated by $\xi = \arg(\partial z_s)$ whilst $e^{i(\varphi + \xi)}$ is the tangential direction to the caustics. In fact, we may alternatively parameterise the critical curves through the tangential direction angle, $\chi = \varphi + \xi$, using $\partial z_s / \partial \bar{z}_s = (\partial z_s) / (e^{-2i\varphi} \bar{\partial} z_s) = e^{2i\chi}$.

Two independent equations of z and \bar{z} in eq. (11) may be transformed again into a polynomial of $p[z(e^{2i\varphi})]$, which can be solved in principle for each $\varphi \in [0, \pi[$. However, unlike the single-plane case, each equation in eq. (11) involves both z and \bar{z} . Once \bar{z} is eliminated, the polynomial $p(z)$ for a generic case is of 20th degree, zeroes of which includes many spurious solutions which need to be checked with the original equation of eq. (11). In fact, the equation for the critical curves can be solved more straightforwardly in polar coordinates (see also Erdl & Schneider 1993) by setting $z = |z|e^{i\theta}$ in $|\partial z_s|^2 = |\partial \bar{z}_s|^2$, which reduces to a quadratic equation on $\cos \theta$ at a fixed $|z|$.

2.3 Magnification sum invariants

For binary lensing in a single plane, Witt & Mao (1995) and Rhie (1997) showed that when a source is inside a caustic (five-image configurations), the sum of signed magnifications $\sigma = \sum_i \mu_i$ is always unity. Based on the method developed by Hunter & Evans (2001, see also Dalal & Rabin 2001; Evans & Hunter 2002), An & Evans (2006) extended this to show that, if the lens equation is given by $z_s = z - \overline{s(z)}$ with an analytic function $s(z)$, then the sum of signed magnifications σ is related to the coefficient of the Laurent series expansion of $[g(z)]^{-1}$ as $z \rightarrow \infty$ such that $[g(z)]^{-1} \simeq \sigma z^{-1} + \mathcal{O}(z^{-2})$. Here $g(z) = z - z_s - \bar{s}[\bar{z}_s + s(z)]$ and $\bar{s}(w) = \overline{s(\bar{w})}$. For the case that $|\lim_{z \rightarrow \infty} s(z)| < \infty$, this then implies $g(z) \sim z$ for a generic source position z_s , and it follows that $\sigma = 1$.

As the deflection term of eq. (7) contains z as well as \bar{z} , their

result is not applicable here. However, Werner (2007) has shown that if the lens equation is given by $z_s = z - s(z, \bar{z})$ where $s(z, \bar{z})$ is a bivariate rational function of (z, \bar{z}) such that the degree of the polynomial in the denominator is greater than that in the numerator (i.e. $s \rightarrow 0$ as $z \rightarrow \infty$), then the holomorphic Lefschetz fixed-point formula (see Griffiths & Harris 1978) from algebraic geometry and topology applies, and subsequently implies that $\sigma = 1$. It is easy to find that eq. (7) indeed meets the condition, and thus the result of Werner (2007) applies here. That is to say, the sum of signed magnifications for six-image configurations should be exactly unity

$$\sum_{i=1}^6 \mu_i = 1, \quad (13)$$

which we have also verified numerically.

3 EXAMPLE LIGHT CURVES

For illustration, we study a scenario where the two lenses have $M_1 = 0.7$ and $M_2 = 0.3$ (the values of m_1 and m_2 will vary as β changes). We set the source distance at 1, and put the first lens is at distance $d_1 = 0.7$. The distance to the second lens (d_2) is varied to see the differences in the light curves. Both lenses are assumed to be static, with the first lens at the origin and the second lens at $z_2 = (0.8, 0.0)$. The source trajectory is horizontal, with the vertical coordinate being 0.03.

In Figs. 1 to 3 we show the magnification patterns and light curves for $d_2 = 0.7, 0.8$, and 0.9 , respectively. At $d_2 = d_1 = 0.7$, we recover the single plane lensing, and there is only one joint caustic on the left. As d_2 increases, the three-dimensionness of lensing increases, and an additional caustic on the right appears. But this is a weak/faint caustic, as a source crosses it, the magnification between the crossing can be very small. For $d_2 = 0.8$, it is 1.15, much smaller than the minimum magnification of 3 for binary lensing in a single plane (Witt & Mao 1995). This is because the faint caustic (on the right) has been strongly deflected by the first lens M_1 , and thus the magnification is lower. This behaviour is known in Lee et al. (1997), although we recovered this without knowing their results.

As d_2 further increases to 0.9, the additional, right-most caustic moves towards the main caustic on the left, and the magnification between the ‘U’-shaped caustics becomes higher, of the order of 2.3, still lower than the minimum value of 3 as in the single-plane binary lensing.

In Appendix B, we quantitatively study the trend of the magnification with β for a source on the x -axis. We show how the behaviour seen in the figures can be understood.

4 SUMMARY AND DISCUSSION

In Galactic microlensing, the probability by microlensing of one star is of the order of $\tau \sim 10^{-6}$, and so the probability of microlensing by two independent stars along the line of sight is $\tau_2 \approx \tau^2 \sim 10^{-12}$. Each year, we monitor about $N_* \sim 2 \times 10^8$ stars, and so the event rate for 3D microlensing is $N_* \times \tau_2/t_E$, where $t_E \approx 0.1$ yr is the typical microlensing event, so this gives about 2×10^{-3} events yr^{-1} , which is quite low. Notice that in principle the farther lens is also lensed by the closer one and its light

curve will be superimposed on that of the background source. However, in practice, this effect may be small because the lenses are expected to be quite faint.

In a single plane Galactic microlensing, the motion of the centre of the mass of the binary can be absorbed into the motion of the source, although the binary rotation (of the order of $\sim 10 \text{ km s}^{-1}$) can still be observed (Albrow et al. 2000; An et al. 2002; Jaroszynski et al. 2005; Hwang et al. 2010; Ryu et al. 2010; for predictions see, Penny, Kerins, & Mao 2011; Penny, Mao, & Kerins 2011). For three-dimensional lensing, the two lenses will move independently with velocities of 100 km s^{-1} , and so the distance between the lenses, and as a result critical curves and caustics, will change as a function of time more rapidly, which may further diversify the light curves. Fig. 4 shows an example of a light curve due to a moving lens. The rate of change in the light curve will depend on the relative motions. In particular, motions parallel to the two lenses may have a bigger impact on the caustics than perpendicular motions. This can be understood analytically in terms of the motions of caustics (see Appendix B).

So far, we have focused on ‘‘resonant’’ microlensing in two planes, it should be mentioned that if the lenses are widely separated then they act as unrelated lenses, and the probability of observing such cases will be comparable to or even larger than the ‘‘resonant’’ microlensing, depending on the separation distributed of close/wide binaries. Indeed, repeated microlensing events due to binary lenses in a single plane have been predicted and observed (Di Stefano & Mao 1996; Di Stefano & Scalzo 1999; Skowron et al. 2009). In this case, the two microlensing peaks will have different timescales but the same colour. They can be differentiated from single-plane binary source events which will have almost the same timescale (modified by the rotation of the binary) and (possibly) different colours (Griest & Hu 1992). The wide-binary lens event in a single plane may be difficult to tell apart from wide three-dimensional microlensing events; the latter, as we argued above, may have much more different timescales than wide single-plane lensing events.

A more likely case for 3D microlensing is cosmological microlensing by stars located in two lens galaxies at different redshifts. We know multiple images can be produced by galaxies at different redshifts, as already seen in the CLASS lens B2114+022 (Chae et al. 2001). In this case, the optical depth for microlensing in each plane is of the order of 0.1–1, and so the two-plane microlensing has a high chance of occurrence. It will be very interesting to explore how the magnification maps are qualitatively different from that in a single microlensing case. Our preliminary study shows that indeed faint caustic crossing events found in this paper also occur, as also found by Lee et al. (1997). It will be interesting to examine this further for specific cases since *LSST*¹ will discover approximately 10^4 new gravitational lenses while simultaneously obtaining their light curves. Some of these (≈ 10 per cent) will be three-dimensional lenses. Notice also that the second lensing galaxy in this case should in principle be ‘‘microlensed’’ by the first galaxy, although in practice, due to the extended size nature of the galaxy, the effect may be small unless there are bright compact sources such as a new supernovae or an active galactic nucleus at the centre of the second galaxy.

¹ www.lsst.org

ACKNOWLEDGMENTS

We acknowledge the National Astronomical Observatories (NAOC) and Chinese Academy of Sciences (CAS) for financial support (SM and JHA). SM acknowledges the Max-Planck Institute for Astrophysics in Garching for travel support where this work was completed. HJW thanks the NAOC and in particular the gravitational lensing and galaxy group for hospitalities during a visit.

REFERENCES

- Albrow M. D., et al., 2000, *ApJ*, 534, 894
 An J. H., et al., 2002, *ApJ*, 572, 521
 An J. H., Evans N. W., 2006, *MNRAS*, 369, 317
 Augusto, P., Browne, I. W. A., Wilkinson, P. N., et al. 2001, *MNRAS*, 326, 1007
 Bernshtein D. N., 1975, *Functional Analysis and Its Applications*, 9, 183
 Browne I. W. A. et al., 2003, *MNRAS*, 341, 13
 Chae K.-H., Mao S., Augusto P., 2001, *MNRAS*, 326, 1015
 Dalal N., Rabin J. M., 2001, *J. Math. Phys.*, 42, 1818
 Di Stefano R., Scalzo R. A., 1999, *ApJ*, 512, 579
 Di Stefano R., Mao S., 1996, *ApJ*, 457, 93
 Erdl H., Schneider P., 1993, *A&A*, 268, 453
 Evans N. W., Hunter C., 2002, *ApJ*, 575, 68
 Griest, K., & Hu, W. 1992, *ApJ*, 397, 362
 Griffiths P., Harris J., 1978, *Principles of Algebraic Geometry*. John Wiley & Sons, New York NY
 Hunter C., Evans N. W., 2001, *ApJ*, 554, 1227
 Hwang K.-H., et al., 2010, *ApJ*, 723, 797
 Jaroszynski M., et al., 2005, *AcA*, 55, 159
 Kochanek C. S., Apostolakis J., 1988, *MNRAS*, 235, 1073
 Kundic, T., Witt, H. J., & Chang, K. 1993, *ApJ*, 409, 537
 Lee M. H., Babul A., Kofman L., Kaiser N., 1997, *ApJ*, 489, 522
 Levine H. I., Petters A. O., Wambsganss J., 1993, *J. Math. Phys.*, 34, 4781
 Mihov B. M., 2001, *A&A*, 370, 43
 Pei, Y. C. 1993, *ApJ*, 403, 7
 Penny M. T., Kerins E., Mao S., 2011, *MNRAS*, 417, 2216
 Penny M. T., Mao S., Kerins E., 2011, *MNRAS*, 412, 607
 Petters A. O., 1995a, *J. Math. Phys.*, 36, 4263
 Petters A. O., 1995b, *J. Math. Phys.*, 36, 4276
 Petters A. O., 1997, *J. Math. Phys.*, 38, 1605
 Petters A. O., Wicklin F. J., 1995, *MNRAS*, 277, 1399
 Rhie S. H., 1997, *ApJ*, 484, 63
 Ryu Y.-H., et al., 2010, *ApJ*, 723, 81
 Skowron J., Wyrzykowski Ł., Mao S., Jaroszyński M., 2009, *MNRAS*, 393, 999
 Sturmfels B., 2002, *Solving Systems of Polynomial Equations* (CBMS Regional Conference Series in Mathematics). American Mathematical Society, Providence RI
 Werner M. C., 2007, *J. Math. Phys.*, 48, 052501
 Werner M. C., An J., Evans N. W., 2008, *MNRAS*, 391, 668
 Witt H. J., 1990, *A&A*, 236, 311
 Witt H. J., Mao S., 1995, *ApJ*, 447, L105
 Witt H. J., Petters A. O., 1993, *J. Math. Phys.*, 34, 4093

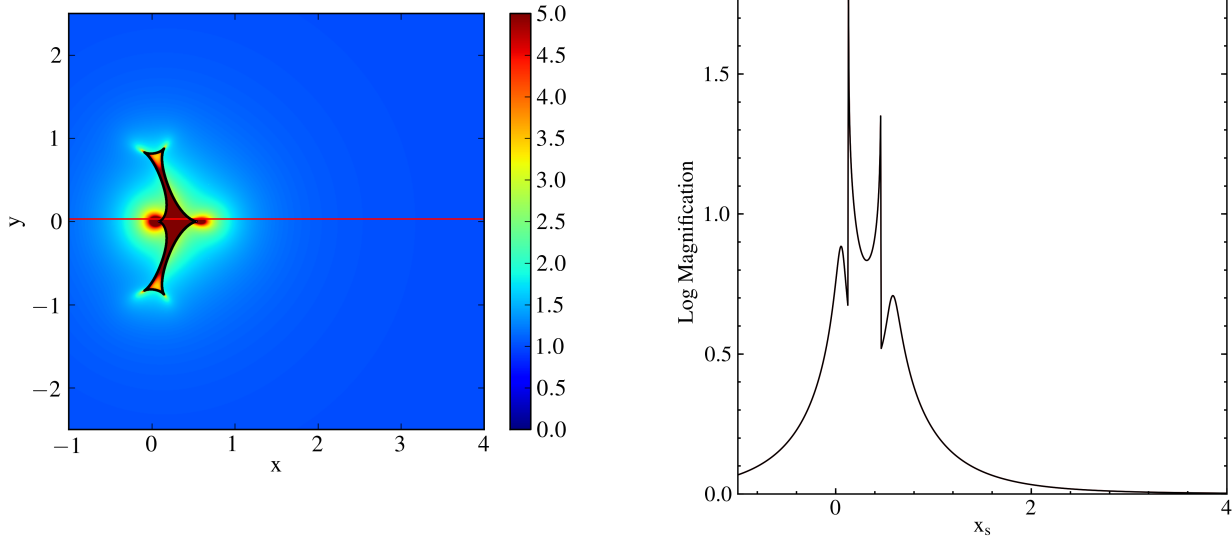


Figure 1. Left: Example caustics, source trajectory and magnification patterns for $d_2 = 0.7$. The two lenses have masses $M_1 = 0.7$ and $M_2 = 0.3$ with the first lens at the origin and the second at $(0.8, 0.0)$. Right: Light curve for the horizontal source trajectory with $y_s = 0.03$ shown in the left.

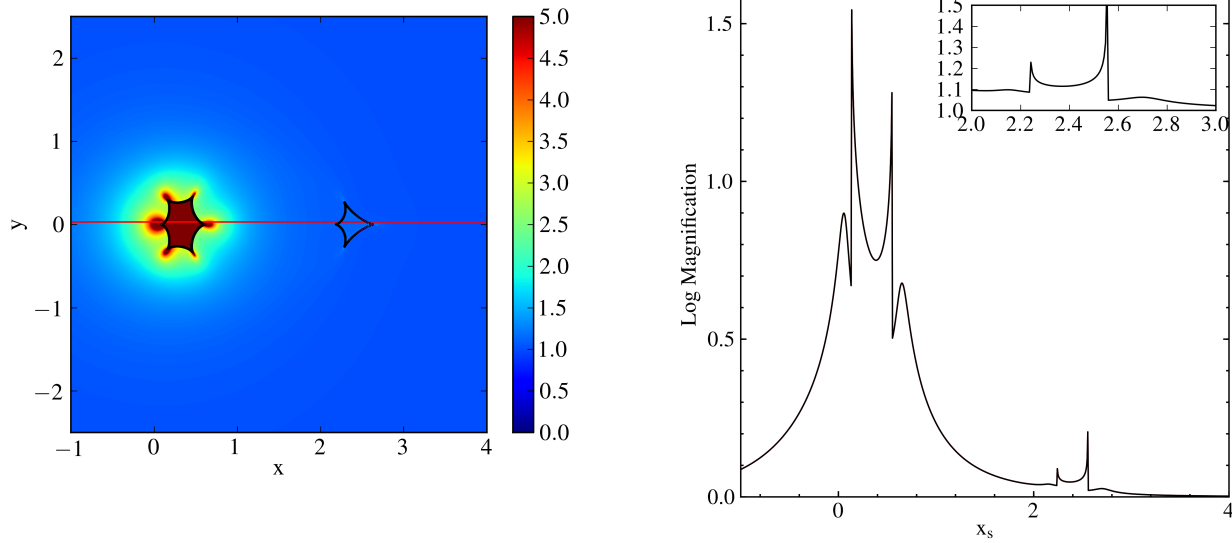


Figure 2. Left: Example caustics, source trajectory and magnification patterns for $d_2 = 0.8$. Right: Light curve for the horizontal source trajectory shown in the left. The inset shows the zoomed in view of the second caustic crossing with magnification on linear scale. Notice that the magnification between the ‘U’-shaped caustic crossing is small, ~ 1.15 .

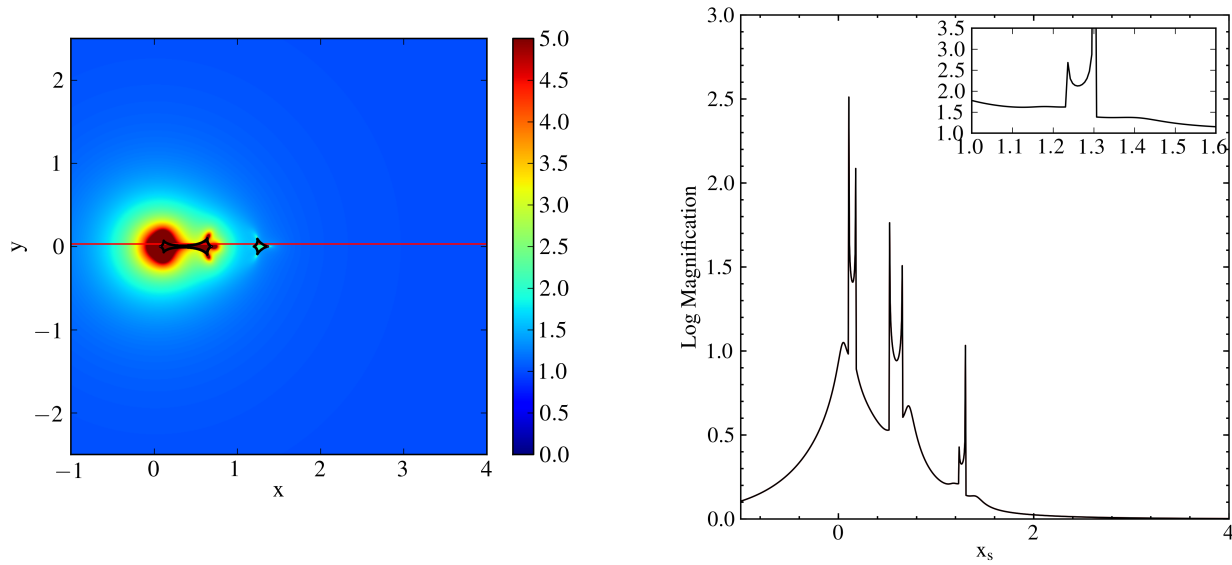


Figure 3. Left: Example caustics, source trajectory and magnification patterns. Right: Light curve for the horizontal source trajectory shown in the left for $d_2 = 0.9$. The inset shows the zoomed in view of the second caustic crossing with magnification on linear scale. Notice that the magnification between the ‘U’-shaped caustic crossing is small, ~ 2.3 , still smaller than the minimum magnification between caustic crossings for binary lenses in a single plane.

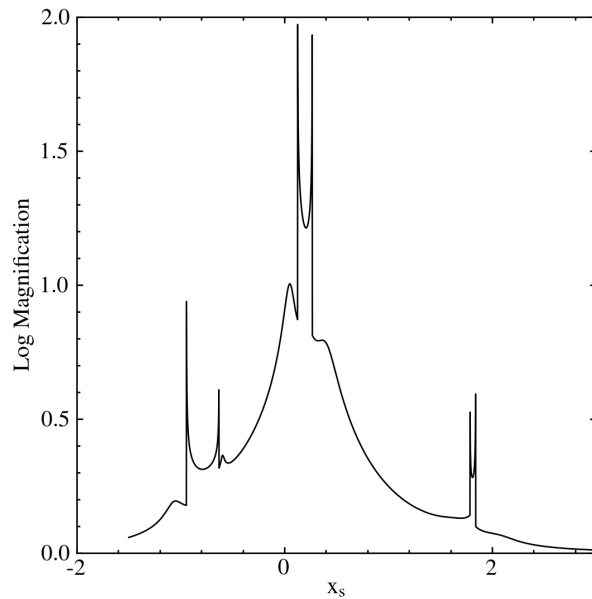


Figure 4. Light curve for a horizontal source trajectory with $y_s = 0.03$, identical to the ones shown in Figs. 1 to 3. The two lenses have masses $M_1 = 0.7$ and $M_2 = 0.3$; the first lens is at a distance of $d_1 = 0.7$ and the second lens at $d_2 = 0.9$ (the same as for Fig. 3). The first lens is fixed at the origin (in projection) while the second lens is moving with $dz_2/dt = 0.54$. As the source moves from -1.5 to 3.5 , the second lens moves from $(-0.55, 0)$ to $(2.15, 0)$.

APPENDIX A: COMPLEX LENS EQUATION

The coefficients for the resultant complex sextic polynomial $g(z; z_s, \bar{z}_s) = \sum_{k=0}^6 a_k z^k$ of the lens equation are given by

$$a_6 = (1 - \beta)(\bar{z}_s - \bar{z}_2)\bar{z}_2\bar{z}_s, \quad (\text{A1a})$$

$$a_5 = m_1(1 - \beta)^2\bar{z}_2\bar{z}_s - m_2(\beta\bar{z}_s - \bar{z}_2)(\bar{z}_s - \bar{z}_2) - [(2 - \beta)z_2 + (1 - 2\beta)z_s](\bar{z}_s - \bar{z}_2)\bar{z}_2\bar{z}_s, \quad (\text{A1b})$$

$$a_4 = [2(1 - \beta)z_2z_s + z_2^2 - \beta z_s^2](\bar{z}_s - \bar{z}_2)\bar{z}_2\bar{z}_s + m_1(1 - \beta)[\bar{z}_2^2z_s - \beta z_2\bar{z}_s^2 - 2(1 - \beta)(z_2 + z_s)\bar{z}_2\bar{z}_s] \\ - m_2[2(z_s + \beta z_2)\bar{z}_2\bar{z}_s - (z_2 + z_s)(\bar{z}_2^2 + \beta\bar{z}_s^2)], \quad (\text{A1c})$$

$$a_3 = (\beta z_s - z_2)(\bar{z}_s - \bar{z}_2)z_2\bar{z}_2z_s\bar{z}_s - m_1^2(1 - \beta)^2(\bar{z}_2z_s + \beta z_2\bar{z}_s) + m_2^2(\beta\bar{z}_s - \bar{z}_2)(z_s - z_2) \\ + m_1m_2[(1 + \beta)(z_2\bar{z}_2 + \beta z_s\bar{z}_s) - 2(\bar{z}_2z_s + \beta^2z_2\bar{z}_s)] - m_2[(z_2\bar{z}_s + \bar{z}_2z_s)(z_2\bar{z}_2 + \beta\bar{z}_s z_s) - 2(1 + \beta)z_2\bar{z}_2z_s\bar{z}_s] \\ + m_1\left\{[(1 - 2\beta)z_2\bar{z}_s - (2 - \beta)\bar{z}_2z_s](z_2\bar{z}_2 + \beta z_s\bar{z}_s) + \beta(z_2\bar{z}_s + \bar{z}_2z_s)^2 + 4(1 - \beta)^2z_2\bar{z}_2z_s\bar{z}_s\right\}, \quad (\text{A1d})$$

$$a_2 = m_1[2(1 - \beta)\bar{z}_2\bar{z}_s - \bar{z}_2^2 + \beta\bar{z}_s^2](\beta z_s - z_2)z_2z_s - m_1^2(1 - \beta)[\beta(\bar{z}_2z_s^2 - z_2^2\bar{z}_s) - 2(1 - \beta)(\bar{z}_2 + \beta\bar{z}_s)z_2z_s] \\ + m_1m_2[2(\bar{z}_2 + \beta^2\bar{z}_s)z_2z_s - (\bar{z}_2 + \beta\bar{z}_s)(z_2^2 + \beta z_s^2)], \quad (\text{A1e})$$

$$a_1 = m_1^3\beta(1 - \beta)^2z_2z_s - m_1^2m_2\beta(\beta z_s - z_2)(z_s - z_2) + m_1^2[(1 - 2\beta)\bar{z}_2 + \beta(2 - \beta)\bar{z}_s](\beta z_s - z_2)z_2z_s, \quad (\text{A1f})$$

$$a_0 = m_1^3\beta(1 - \beta)(\beta z_s - z_2)z_2z_s. \quad (\text{A1g})$$

The degree of the polynomial may be reduced if $a_0 = 0$ or $a_6 = 0$. The case $\beta = 0$, which corresponds to the single plane lensing, results in $a_0 = 0$ and thus z factors out of the polynomial leaving a quintic quotient. Since $z = 0$ is not a solution of the lens equation, the maximum number of images of a single plane binary lensing is five. If $\beta = 1$ on the other hand, then both $a_0 = a_6 = 0$ and so the polynomial becomes a quartic times z , leaving the maximum four images. Similar reductions of the polynomial to a quartic are also possible for $z_2 = 0$ (i.e. two lenses being aligned) or the special source positions corresponding to $z_s = 0$, $z_s = z_2$ or $z_s = \beta^{-1}z_2$. However they can be understood as particular cases of $z_s = \zeta z_2$ with $\zeta \in \mathbf{R}$, which shall be discussed next.

In principle, without any loss of generality, the real axis can be chosen such that the complex position of second deflector z_2 is positive real (i.e. $z_2 = \bar{z}_2 > 0$). The case that both the source and the second deflector are located on the real axis on the other hand represents the physical scenario that the observer, two deflectors, and the source are all co-planar. A geometric argument concerning this case indicates that there must be four images along the real axis as well. These are found with eqs. (7) or (8) by setting $z = \bar{z}$ and $z_2 = \bar{z}_2$, which results in a quartic polynomial equation $g_4(z) = 0$ where

$$g_4(z) = z^4 - (z_2 + z_s)z^3 + [z_2z_s - (\beta + 1)m_1 - m_2]z^2 + m_1(z_2 + \beta z_s)z + \beta m_1^2 \\ = (z^2 - z_s z - m_1 - m_2)(z^2 - z_2 z - \beta m_1) - m_2(z_2 z + \beta m_1). \quad (\text{A2})$$

Given real $z_s, z_2 \in \mathbf{R}$ and positive $\beta, m_1, m_2 > 0$, the equation $g_4(z) = 0$ possesses four real solutions $z \in \mathbf{R}$, which is shown as follows. Let us suppose that z_{\pm} are two zeroes of $z^2 - z_2 z - \beta m_1$ (i.e. corresponding to $w = z_2$), namely,

$$z_{\pm} = \frac{z_2 \pm \sqrt{z_2^2 + 4\beta m_1}}{2} = \pm \frac{z_2}{2} \left[\left(1 + \frac{4\beta m_1}{z_2^2} \right)^{1/2} \pm 1 \right], \quad (\text{A3a})$$

and thus $z_- < 0 < z_+$ for $z_2 > 0$ (the following is still valid for $z_2 < 0$ with $z_+ \leftrightarrow z_-$). Next $g_4(0) = \beta m_1^2 > 0$ whilst

$$g_4(z_{\pm}) = -m_2(z_2 z_{\pm} + \beta m_1) = - \left[\left(1 + \frac{2\beta m_1}{z_2^2} \right) \pm \left(1 + \frac{4\beta m_1}{z_2^2} \right)^{1/2} \right] \frac{m_2 z_2^2}{2} < 0. \quad (\text{A3b})$$

Since $g_4(z)$ is a monic quartic, the intermediate value theorem together the fundamental theorem of algebra indicates that $g_4(z) = 0$ has four real solutions, – one each in the intervals, $]-\infty, z_-[$, $]z_-, 0[$, $]0, z_+[$, and $]z_+, \infty[$ – all of which corresponds to true image positions. The remaining two off-axis solutions, if any, must still be the zero of the sextic $g(z; z_s, \bar{z}_s)$ with $z_s = \bar{z}_s$ and $z_2 = \bar{z}_2$, which is in fact divisible by $g_4(z)$, that is to say, $g(z; z_s, \bar{z}_s) = g_4(z)g_2(z)$ where

$$g_2(z) = (1 - \beta)(z_s - z_2)z_s z_2 z^2 + [m_1(1 - \beta)^2 z_s z_2 + (z_2 z_s - m_2)(\beta z_s - z_2)(z_s - z_2)]z + m_1(1 - \beta)(\beta z_s - z_2)z_s z_2. \quad (\text{A4})$$

Since $z_s, z_2 \in \mathbf{R}$, the coefficients of $g_2(z)$ are all real, and its two zeroes are either both real or a pair of complex conjugates. Next, we find $f(z_a, z_b) = 0$ where z_a and z_b are the pair of zeroes of $g_2(z)$ and f is the polynomial in eq. (8). In other words, the complex conjugate roots of $g_2(z) = 0$ are true off-axis images whereas its non-degenerate real zeroes are spurious solutions. Consequently, along the real axis, the source lies inside, on, and outside caustics if the discriminant of $g_2(z)$ is negative, zero, and positive respectively. Some results for the corresponding magnifications are explored in the next section.

If $z_2 = 0$ (that is, two lenses are aligned),

$$g_4(z) = z^4 - z_s z^3 - \mathcal{M}z^2 + \beta m_1 z_s z + \beta m_1^2, \quad g_2(z) = -\beta m_2 z_s^2 z \quad (\text{A5})$$

where $\mathcal{M} = (1 + \beta)m_1 + m_2$. Note $g_2(z)$ is now linear and its sole zero $z = 0$ is again not a image position. Provided that $z_s \neq 0$, the number of images for two perfectly aligned lenses is therefore four (Werner et al. 2008). All four images for an arbitrary source position z_s are found to be $z = r e^{i\phi}$ where $\phi = \arg(z_s)$ – i.e. $z_s = |z_s| e^{i\phi}$ – and r being the root of $r^4 - |z_s| r^3 - \mathcal{M}r^2 + \beta m_1 |z_s| r + \beta m_1^2 = 0$. Finally the solution for $z_s = 0$ case, i.e. $r^4 - \mathcal{M}r^2 + \beta m_1^2 = 0$ corresponds the radii of two Einstein rings (Werner et al. 2008).

APPENDIX B: THE MAGNIFICATION OF A SOURCE ALONG THE REAL AXIS

Assuming $z_2 \in \mathbf{R}$, we can evaluate the magnification for the source along the real axis ($z_s \in \mathbf{R}$). As noted, the quartic equation $g_4(z) = 0$ yields four images on the real axis; whereby i) two positive parity images and two negative parity images if the source is outside caustics or ii) three negative parity and one positive parity images if the source is inside caustics. On the other hand, the quadratic equation $g_2(z) = 0$ for the source inside caustics yields a pair of positive-parity off-axis images of the equal magnification that are symmetric about the real axis. The real axis passes caustics through its cusp points. As the source moves along the real axis and enters the caustic, one positive-parity on-axis image crosses the critical curve and turns into a negative-parity one whilst two positive-parity off-axis images emerge from the same critical point passed by the on-axis image. Upon the exit of the source from the caustic, the reverse process (viz. merging of two positive-parity off-axis images and one negative-parity on-axis image into one positive-parity on-axis image on the critical point) takes place.

B1 A source inside caustics

The image of positive parity on the real axis is mostly very faint inside the *bright* caustic. However, the situation changes inside the *faint* caustic. In this case the off-axis magnification becomes $\mu \sim 0.1$ and the on-axis magnification of the positive parity becomes $\mu \geq 1$. Next, we further restrict ourselves to the case $M_1 = M_2$ so that $m_1 = 1/(2 - \beta)$ and $m_2 = (1 - \beta)/(2 - \beta)$. However, we note here that we can partly expand our results to unequal masses M_1 and M_2 because $\alpha = 1 - \beta$ may be scaled like $\alpha' = \alpha M_2/M_1$ as long as $0 < \alpha, \alpha' < 1$ holds. Applying the resultant method to the magnification for eliminating z and \bar{z} , we express the magnification as a function of z_s . For the two positive-parity images resulting from $g_2(z) = 0$, we find

$$\mu_1 = \mu_2 = (1 - \beta)^2 (\beta z_s - z_2)^2 z_2^2 [P_6(z_s)]^{-1} \quad (\text{B1})$$

where $P_6(z_s) = \sum_{k=0}^6 c_k z_s^k$ is a sextic polynomial of z_s whose coefficients are given by

$$c_6 = -(2 - \beta)^2 \beta^2 z_2^2 \quad (\text{B2a})$$

$$c_5 = 2(2 - \beta)\beta z_2 [\beta(1 - \beta)(1 + z_2^2) + 2z_2^2] \quad (\text{B2b})$$

$$c_4 = -\beta^2(1 - \beta)^2 - 2\beta(2 - \beta)(1 - \beta)(1 + 3\beta)z_2^2 - (2 - \beta)^2(1 + 4\beta + \beta^2)z_2^4 \quad (\text{B2c})$$

$$c_3 = 2z_2 [2\beta(1 - \beta)^2 + 2(4 - \beta^2)(1 - \beta)z_2^2 + (2 - \beta)^2(1 + \beta)z_2^4] \quad (\text{B2d})$$

$$c_2 = -z_2^2 [2(1 - \beta)^2(2 + \beta) + 2(2 - \beta)(1 - \beta)(1 + 3\beta)z_2^2 + (2 - \beta)^2 z_2^4] \quad (\text{B2e})$$

$$c_1 = 2(1 - \beta)z_2^3 [2(1 - \beta) + (2 - \beta)z_2^2] \quad (\text{B2f})$$

$$c_0 = -(1 - \beta)^2 z_2^4 \quad (\text{B2g})$$

Let μ_3 be the magnification of the positive-parity on-axis image and μ_4, μ_5 and μ_6 the magnification of the negative-parity ones which are located on the real axis. Then using eq. (13) and $\mu_1 = \mu_2$, we obtain an expression for the total magnification

$$\mu_{\text{tot}} = \sum_{i=1}^6 |\mu_i| = \sum_{i=1}^3 \mu_i - \sum_{i=4}^6 \mu_i = 2 \sum_{i=1}^3 \mu_i - 1 = 4\mu_1 + 2\mu_3 - 1, \quad (\text{B3})$$

which is the key equation to understand the different behaviour of the two caustics. Whilst inside the *bright* caustic $\mu_1 \geq 1$ and therefore $\mu_{\text{tot}} > 3$, we have inside the *faint* caustic $\mu_3 \geq 1$ and therefore $\mu_{\text{tot}} > 1$.

For the four on-axis images we can also derive a polynomial (of the 4th degree) for the magnification, which is too long to be presented here. However, to obtain the total magnification we only need to estimate the magnification of the single positive-parity image, which turns out always to be very faint inside the *bright* caustic. For small β we obtain

$$\mu_3 \approx \frac{(1 - \beta)^4 \beta^6}{16z_2^8 + 64\beta z_2^6 (2 - z_s z_2 + z_2^2) + \dots} \ll 1 \quad (\text{B4})$$

Note that for $\beta \ll 1$ and $\beta \approx 1$ the numerator becomes extremely small. Since μ_3 can be neglected we can derive the minimum magnification from the equation above. μ_1 has a minimum when $2\beta P_6(z_s) = (\beta z_s - z_2) P_6'(z_s)$ holds. For the *faint* caustic μ_3 takes the dominant part and the images of negative parity becomes rather faint ($2\mu_1 < |\sum_{i=4}^6 \mu_i| \ll 1$). For the minimum magnification inside the *faint* caustic we can write $d\mu_{\text{tot}}/dz_s = 4(d\mu_1/dz_s) + 2(d\mu_3/dz_s) = 0$ by using eq. (B3). Since $\mu_{\text{tot}} \approx 2\mu_3 - 1$ for this case each derivative must vanish at the approximate same location z_s . Therefore we can apply $2\beta P_6(z_s) = (\beta z_s - z_2) P_6'(z_s)$ for the location of the minimum magnification inside the *faint* caustic as well.

Finally we note that the caustic, i.e. cusps intersects with the real axis when $P_6(z_s) = 0$. In this case we obtain infinite magnification for a point source. The real solutions give the range where 6 images can occur. The two caustic may merge if P_6 has a double solution or if $P_6(z_s) = 0$ and $P_6'(z_s) = 0$ holds. Using these two equations we obtain the condition when the two caustics may touch and merge.

$$\begin{aligned} & (2 - \beta)^6 z_2^{12} + 2(2 - \beta)^5 (-3 + 7\beta) z_2^{10} + (2 - \beta)^4 (-15 - 3\beta + 70\beta^2 - 63\beta^3 + 27\beta^4) z_2^8 \\ & - (2 - \beta)^3 (1 - \beta) (8 + 65\beta + 207\beta^2 - 513\beta^3 + 297\beta^4) z_2^6 - (2 - \beta)^2 (1 - \beta)^2 \beta (40 + 595\beta - 758\beta^2 + 27\beta^3) z_2^4 \\ & + 8(2 - \beta) (1 - \beta)^3 \beta^2 (-39 + 31\beta) z_2^2 + 16(1 - \beta)^4 \beta^3 = 0 \quad (\text{B5}) \end{aligned}$$

The change in the number of caustics and cusps for the simple binary lens with shear was first studied by Witt & Petters (1993).

B2 The velocity of the faint caustic

It is necessary to estimate the motion of the *faint* caustic since the two point masses are usually not gravitationally bound to each other for $\beta > 0$. Therefore we have to consider some projection effects due to the motion of the second point mass $z_2(t)$. Assume that the second mass has a relative motion $v_2 = dz_2/dt$. To compute the velocity along the entire caustic one may follow Kundic et al. (1993). This method allows for general deflectors to compute the dependence of the velocity of each caustic point on the motion of the stars, i.e. point masses. For a full analytical treatment this method turns out to be rather complicated, however for a rough estimate we may inspect the polynomial P_6 above. The solutions of $P_6(z_s) = 0$ yield the positions of the cusps along the real axis. Using now eqs. (B2a) and (B2b) we can write

$$\sum_{i=1}^6 z_{\text{cusp},i} = -\frac{c_5}{c_6} = \frac{2z_2[2 + \beta(1 - \beta)(z_2^{-2} + 1)]}{(2 - \beta)\beta} = 2 \left(\frac{1 + \beta}{\beta} z_2 + \frac{1 - \beta}{2 - \beta} \frac{1}{z_2} \right) \quad (\text{B6})$$

where $z_{\text{cusp},i}$ denotes 4 real solutions of the position of the cusps on the real axis and two complex spurious solutions. We assume here that we have at least two separate caustics. i.e. 4 cusps on the real axis (cf. Fig. 2). Assuming now the second point mass moves along the real axis we may write

$$\sum_{i=1}^6 \frac{dz_{\text{cusp},i}}{dt} = 2 \left(\frac{1 + \beta}{\beta} - \frac{1 - \beta}{2 - \beta} \frac{1}{z_2^2} \right) v_2, \quad (\text{B7})$$

For small β the first term dominates which gives us the approximate velocity of the *faint* caustic. Since we have two cusp position we find $v_{\text{caustic}} \approx v_2/\beta$ and $z_{\text{cusp}} \approx z_2/\beta$ to the first order. The other solutions remain small ~ 1 . This is verified numerically and by inspecting c_0/c_6 which yields the product of all six solutions. This means for small β the *faint* caustic may move rather rapidly across the source plane so that the chance to observe a complete caustic crossing is much smaller than that for moderate β . Motions along the y -axis must be of the order of dz_2/dt due to the rotation invariance of the caustics around the origin for $z_2 = r_2 e^{i\varphi_2}$.